

Assessing the impact of process parameters on lattice structure manufacturing defects through micro-CT scanning

Minsol Park^{1*}, Martin Phillip Venter², and Anton Du Plessis^{3, 4}

¹ Department of Mechanical and Mechatronics Engineering, University of Stellenbosch, South Africa, 26724545@sun.ac.za

² Department of Mechanical and Mechatronics Engineering, University of Stellenbosch, South Africa, mpventer@sun.ac.za

³ Department of Physics, University of Stellenbosch, South Africa, anton2@sun.ac.za

⁴ Object Research Systems Inc, Montreal, Canada, aduplessis@theobjects.com

Abstract. In this study, we examined the impact of process parameters on the manufacturing defects in micro-strut lattice structures produced via Laser Powder Bed Fusion (L-PBF). By intentionally varying parameters like laser power and layer thickness, we investigated how these changes affect internal pores, surface roughness, and geometry discrepancies. To quantify these defects, micro-CT (Computed Tomography) scanning analysis was utilised. Our findings demonstrate that manufacturing defects in lattice structures are highly sensitive to variations in process parameters. The results of this study shed light on how process parameters can be adjusted to improve the quality of micro-strut lattice structures.

1 Introduction

Additive manufacturing (AM) has revolutionised the manufacturing industry by providing greater design freedom, replacing traditional subtractive manufacturing. AM builds a part layer-by-layer, and one of the most popular techniques used is L-PBF. In L-PBF, a laser serves as the energy source to selectively melt the powdered material in the desired area, resulting in the creation of a three-dimensional structure [1]. Due to its high accuracy and reproducibility, L-PBF is extensively used in the production of metallic parts with intricate geometries, which are challenging for traditional manufacturing methods [2]. Lattice structures are among the promising applications of L-PBF, offering high strength-to-weight ratios, design flexibility, and customisable mechanical properties, making them highly attractive for various applications [3]. However, manufacturing defects in these structures are inevitable, which can impair the quality and mechanical performance of the lattice structures [4, 5]. These manufacturing defects arise from the unstable thermodynamic state of the melt pool area [1], which is determined by the process parameters. Thus, researchers have extensively investigated the influence of process parameters on manufacturing defects to improve the quality of lattice structures.

* Correspondant author: 26724545@sun.ac.za

Kasperovich *et al.* [6] studied the correlation between the internal porosity in Ti6Al4V alloys produced with L-PBF and process parameters, reporting that optimising process parameters can minimise internal porosity. Egan *et al.* [7] reported that increasing laser power and exposure time increases the strut diameter and volume fraction of diamond lattice structures. Fox *et al.* [8] conducted a study to investigate the influence of process parameters on the surface roughness of overhanging structures. Their findings revealed that high inclination and low laser power can result in the formation of partially melted powder particles, which can cause irregular surface morphology.

Micro X-ray CT is a powerful non-destructive analysis tool that is widely used for the material characterisation of AM metals. It provides an opportunity to detect both external and internal manufacturing defects through the reconstruction of model 3D digital image. A review [9] provides an excellent summary of the technology application of CT in AM.

Yan *et al.* [10] conducted a study to evaluate the manufacturability and performance of gyroid lattice structures using CT scan results. Their results showed that CT scanning can effectively identify defects and measure geometrical features, such as porosity and strut thickness, which is critical in assessing the quality of the lattice structure.

Du Plessis [11] used CT scan analysis to investigate the effects of process parameters on the porosity of Ti6Al4V alloys produced with the L-PBF method. The study found that the internal porosity is strongly influenced by the laser power and scan speed. Du Plessis *et al.* [12] extended the study to examine the lattice structure's microporosity of gyroid lattice structures produced at various laser powers. Their results revealed that the lack of fusion pores can critically deteriorate fatigue performance, while keyhole pores at a low level are not critical to fatigue performance in high-cycle loading experiments.

Despite the considerable amount of research on process parameters, manufacturing defects, and lattice structures, our knowledge of the relationship between process parameters and manufacturing defects on micro-strut lattice structures remains limited. While non-ideal parameters are known to produce increased porosity and surface roughness, how this influences lattice structures in practice is still not well described. This study aims to enhance our understanding of how process parameters, specifically layer thickness and laser power, impact the incidence and severity of manufacturing defects on diamond lattice coupons through CT scan analysis.

2 Methodology

The micro-strut lattice coupon samples were modeled using the default diamond lattice design offered by the software *Materialise Magics 25*. Each sample consisted of 10-unit cells in each dimension with a size of 20x20x20 mm and a 20 % volume fraction of lattice structure measured using CAD software *AutoDesk Fusion 360*. A manufacturing process was conducted utilising a default hard scraper with the following parameters: a scan speed of 1.2 m/s, a spot size of 100 μm , and a hatch distance of 0.15 mm. The lattice coupons were produced using Ti6Al4V powders with five different process parameter settings that varied in laser power (210, 280, and 360 W) and layer thickness (30, 60, and 90 μm). Each sample was named based on its laser power (P) and layer thickness (T). For instance, P280-T30 represents the sample with a laser power of 280W and a layer thickness of 30 μm . In total, five sample sets were considered, with P280-T30 selected as the reference sample since this corresponds to the recommended process parameter set for the machine used – the EOS M290, located at Executive Engineering, South Africa. The process parameters were then modified from the reference sample, with the layer thickness changed to 60 μm (P280-T60) and 90 μm (P280-T90), and the laser power adjusted to 210 W (P210-T30) and 360W (P360-T30).

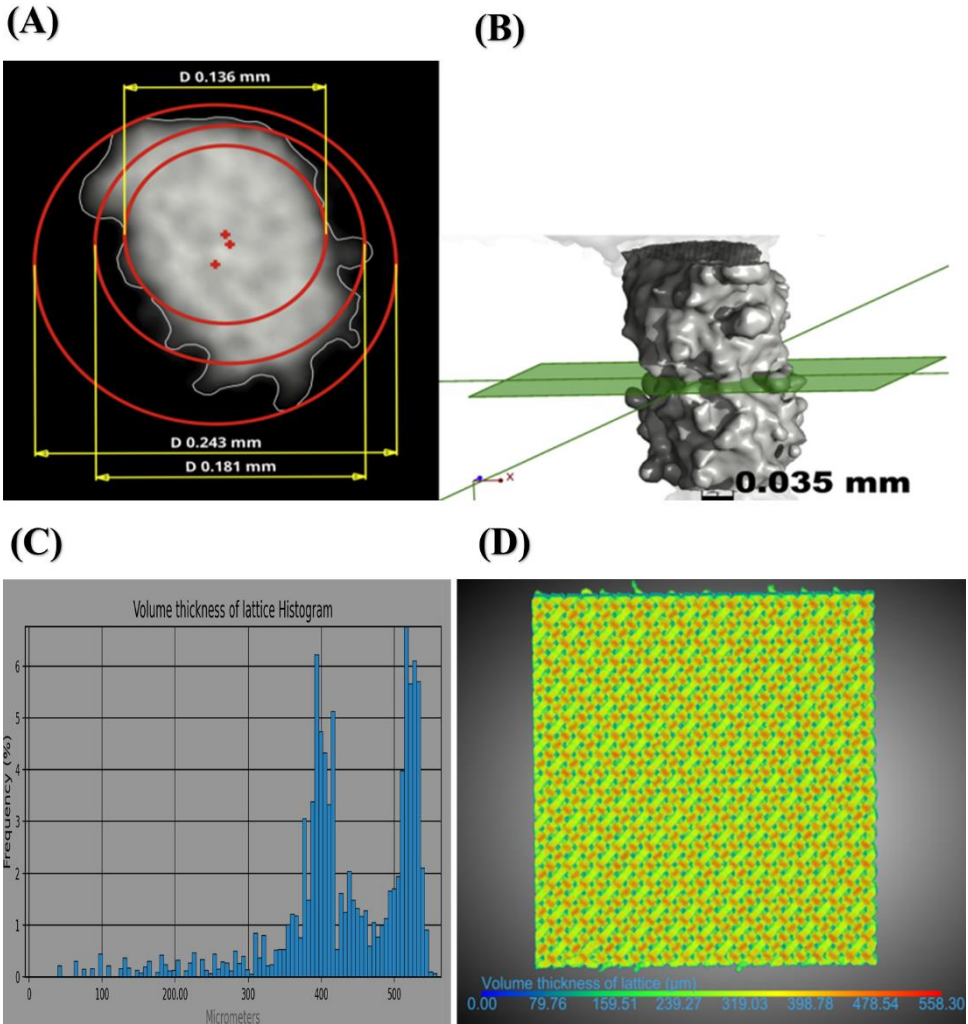


Fig.1. Volume thickness mapping analysis using *Dragonfly* : (A) different circle fitting methods inscribed (smallest circle), Gaussian least-square (medium size circle), and circumscribed (biggest circle) fitting methods [2], (B) example of a circle fitting method on individual strut [2], (C) histogram of volume thickness mapping (D) front view of volume thickness mapping.

The CT scan was conducted at the CT scan facility at Stellenbosch University using a 0.5 mm copper beam filter [13]. The CT scan settings included a voxel size of 25 μm , a voltage of 130 kV, a current of 100 μA , and a total of 3000 images acquired during the scanning process. To evaluate the geometrical discrepancy between the as-designed model and printed lattice coupons, the strut thickness and node thickness were obtained using volume thickness mapping (Fig.1). The volume thickness map provides thickness values for each point/voxel in the volume [14], which correspond to the maximum measure, equating to the maximal-inscribed sphere, which is essentially the smallest circle depicted in Fig.1A. In the present study, the volume thickness map serves as a statistical representation of the thickness of the individual local regions of micro-struts in lattice structures. Fig.1C shows an exemplary statistical histogram of volume thickness mapping. Two definite peak points can be observed from the histogram, around 400 and 520 μm . These two peaks represent the thickness of the

struts and nodes, respectively. This can also be seen in Fig.1D, where most of the struts are yellowish (319-398 μm) and the strut connection points are red (479-558 μm).

The internal porosity was quantified by using Otsu's method [15] to create regions of interest for the pore spaces and material regions based on the given threshold intensity. Firstly, the CT-scanned lattice was extracted from the dark background using binary thresholding (Fig. 2A) and then the internal pores were isolated by extracting the low-intensity dark grey pixels within the lattice structure (Fig. 2B).

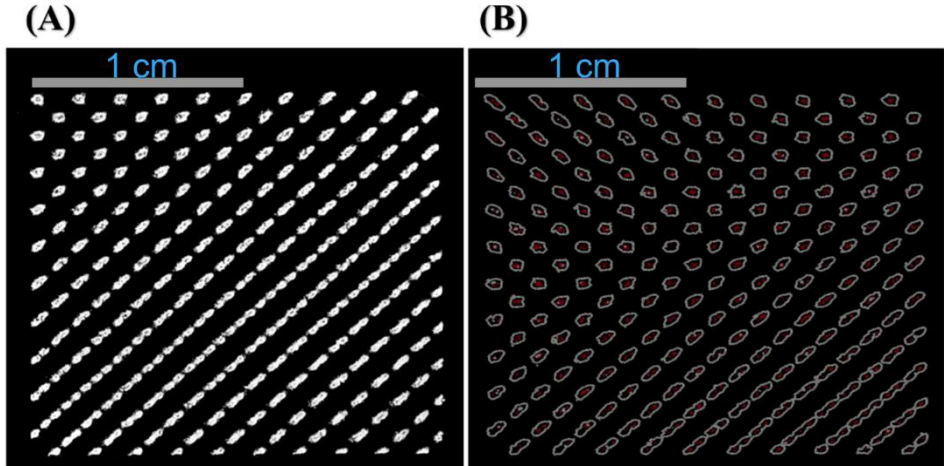


Fig.2. (A) Cross-sectional view of lattice structure isolated by Otsu-method (B) Cross-sectional view of internal pores (red) and lattice surface (grey) separated by Otsu-method.

The surface roughness was quantified using a MATLAB code StrutSurf proposed by Oosterbeek R and Jeffers J [16] which enables the analysis of the strut morphology of the AM lattice structures. The CT scan images in binary format are generated using Dragonfly and exported to StrutSurf. The software allows the strut morphology of a selected single strut of the lattice structure (Fig.3). The surface roughness indicating parameter (R_a) of the overall lattice structure was estimated by obtaining the mean of the statistical data from 30 different struts.

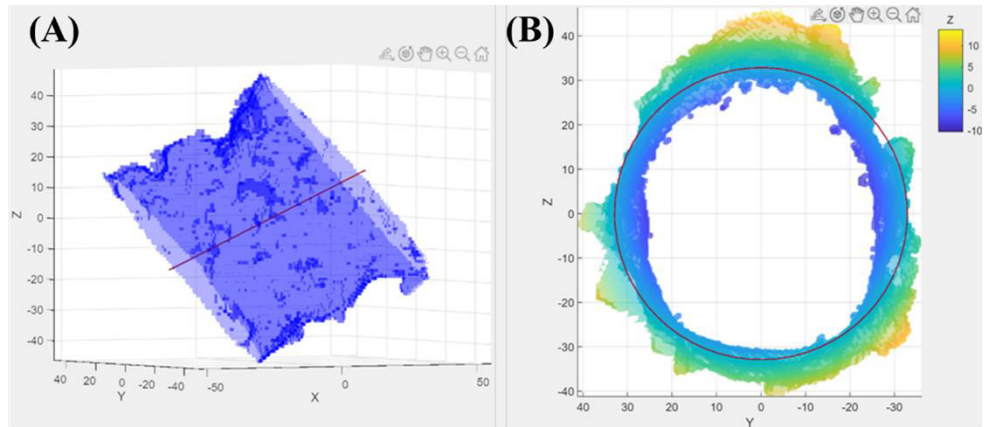


Fig.3. StrutSurf surface morphology analysis : (A) selection of a single strut of a lattice structure and (B) cross-sectional view of a selected lattice strut.

3 Results and discussion

3.1 Geometrical discrepancies

The lattice parameters obtained from CT scan analysis results are presented in Table 1. To better understand the manufacturing defects, a careful study of the CT scan data was performed image by image, as quantified values alone may not provide a complete understanding. Fig. 4 shows typical cross-sectional images of the sub-region of five different samples, with the overlapping of the as-designed model mesh (white solid line). From Fig.4, the overall thickness of lattice structures appears to be smaller than the as-designed model. The node and strut thickness between lattice coupons were compared to the selected reference sample P280-T30. The analysis of CT scan data showed that the strut thickness decreases with increasing layer thickness (Fig.5), which is likely due to the variation in the size of the melt pool area [1]. Samples P280-T60 and P280-T90 had 2 % and 5 % lower strut thickness, respectively than sample P280-T30. This indicates that using higher layer thicknesses can lead to thinner strut thicknesses. No clear correlation was found between node thickness and layer thickness. Sample P280-T60 had a 4 % higher node thickness, while sample P280-T90 had a 4 % smaller node thickness than sample P280-T30. This suggests the parameters recommended to be optimal for solid materials found in the literature [11] are not necessarily optimal for lattice structures. However, the differences in thickness values fall within the reproducibility of 5 %, which makes it difficult to deduce a correlation between node thickness and layer thickness.

Table 1. Manufacturing defect parameters of lattice structures produced with different process parameters, including strut thickness, node thickness, internal porosity, and R_a . R_a values are presented in the mean values with one standard deviation.

	P280-T30	P280-T60	P280-T90	P210-T30	P360-T30
Parameter	Recommend	thickness	thickness	Power	Power
		60	90	80%	120%
Strut Thickness (μm)	363	357	344	326	386
Node Thickness (μm)	447	463	431	399	504
Internal Porosity (%)	2.17	0.27	-	10.8	0.25
R_a (μm)	17.3 (2.3)	22.1 (3.0)	20.7 (4.4)	21.2 (4.8)	25.5 (4.5)

The effect of variation in laser power on the strut thickness, and node thickness seems more crucial compared to the change in the layer thickness. Sample P210-T30 has a 10 % lower strut thickness, and 11 % lower node thickness compared to sample P280-T30. In the L-PBF process, laser power determines the size of the melt pool area. With low laser power input, fewer powders in the scan path are completely melted, creating a smaller melt pool area and thinner struts and nodes, while the larger melt pool area forms with the excess in the laser power input enlarges the size of struts and nodes [2]. Sample P360-T30 sample has a 6 % greater strut thickness and 13 % greater node thickness than that of compared to the P280-T30.

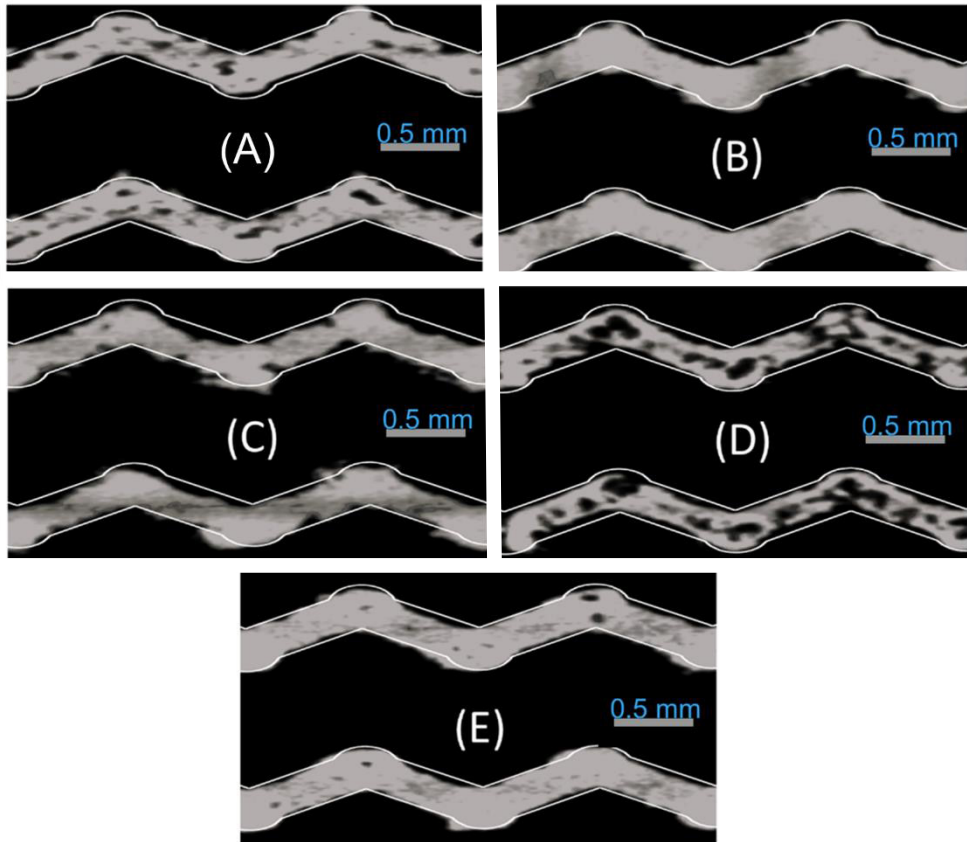


Fig.4. CT-Scanned cross-sectional view of the struts (A) P280-T30, (B) P280-T60, (C) P280-T90, (D) P210-T30, (E) P360-T30, where the white solid lines show the as-designed lattice model.

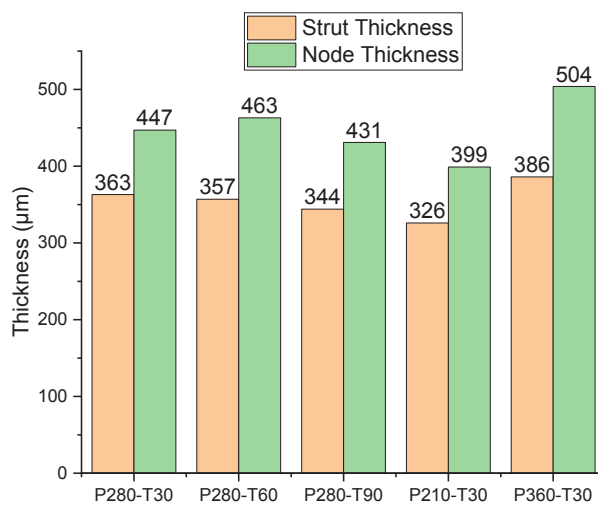


Fig.5. Bar graphs of strut thickness, and node thickness of lattice structures.

3.2 Internal porosity

The internal porosity of lattice coupons ranges from 0.25 % to 10.8 %, as presented in the bar graph (Fig.6). The internal porosity values of sample P280-T90 were unobtainable due to the poor quality of the CT scan. Among the five samples, the most porous sample is sample P210-T30, which is produced with low laser power input. This is due to the lack of fusion and incomplete melting of powders during the fabrication process, resulting in the formation of internal pores, as shown in Fig.4 D. The internal porosity of sample P210-T30 is approximately 5 times greater than that of the second most porous sample P280-T30. Conversely, key-hole pores are observed in sample P360-T30 (Fig.4 E), which are the result of the excessive power input.

The combination of layer thicknesses ranging from 30 to 90 μm and a laser power of 280 W appears to result in the formation of a lack of fusion pores. Sample P280-T30 exhibited a higher level of internal porosity compared to the samples produced with a thicker layer, P280-T60 and P280-T90. This finding contradicts the trend observed in bulk AM metals, where an increase in layer thickness is known to lead to more internal pores due to a lack of fusion. It indicates that small-scaled lattice structures respond differently from bulk materials to changes in layer thickness as well as other process parameters such as laser power or scan speed [11]. It is evident that the heat input becomes excessive when applying the same parameters used for bulk materials to fabricate lattice structures. This phenomenon arises from the significantly reduced heat dissipation capacity, or heat sink, inherent in lattice structures as compared to solid materials. Furthermore, the heightened sensitivity of lattice structures to various process parameters plays a substantial role in their distinct responsiveness. This sensitivity is particularly notable due to the use of shorter hatch tracks during scanning over significantly smaller areas, resembling isolated islands within a vast sea, as depicted in Fig. 2B. Based on the CT scan images (Fig.4C), it can be speculated that sample P280-T90 may have higher levels of internal porosity than P280-T60. Although the results suggest that a layer thickness of 60 μm is an optimal parameter selection for minimising internal porosity in the lattice structure, it is important to note that this is based on a limited sample size of only three lattice samples, with a parameter range of 30-90 μm (incrementing by 30 μm). Therefore, further research is necessary to better understand the relationship between layer thickness and internal porosity.

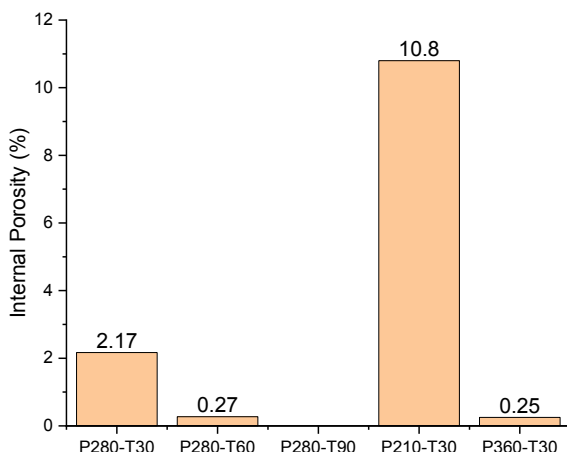


Fig.6. Bar graph of internal porosity of lattice structures.

3.3 Micro CT-scan analysis-surface roughness

The current study also examines the impact of variations in laser power and layer thickness on the surface morphology of lattice structure struts. The surface roughness of the lattice struts was evaluated both qualitatively through CT scan images (Fig.7) and quantitatively through mean R_a values gathered from statistical data in Table 1. The CT scan images demonstrated a distinct difference in surface morphology between upward-facing and downward-facing surfaces for all samples, which aligns with findings in the literature [2]. Specifically, sample P280-T30 exhibited a relatively smoother surface compared to the other samples, while the surface morphology of the remaining samples appeared similar and was challenging to assess qualitatively.

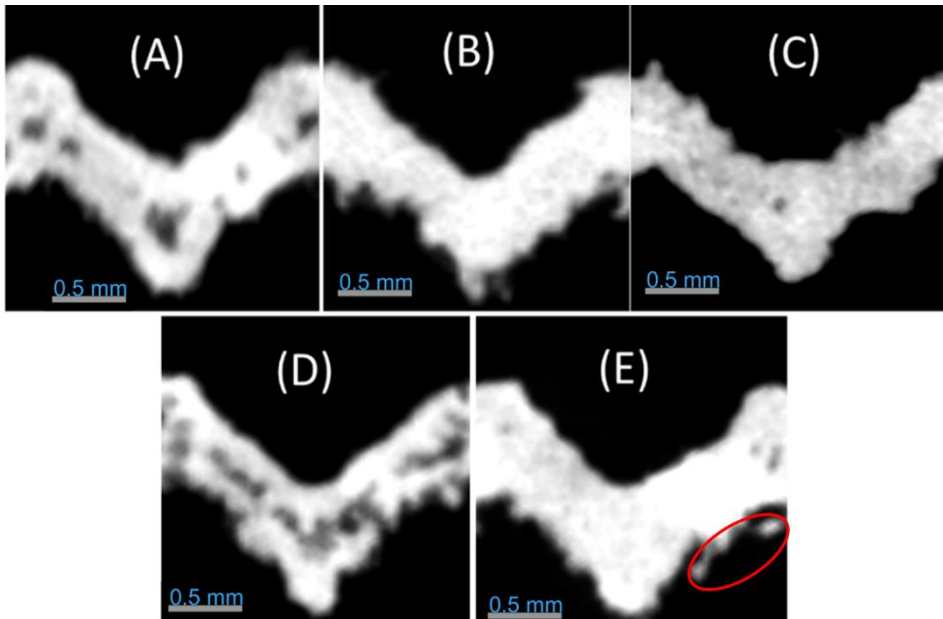


Fig.7. CT-Scan images showing roughness of the struts (A) P280-T30, (B) P280-T60, (C) P280-T90, (D) P210-T30, (E) P360-T30 where the red ellipse mark shows the overhanging feature.

Fig. 8A shows Box-Wisker diagrams that provide a summary of the statistical data for the R_a value. The data sets exhibit negative skewness except for sample P360-T30, which suggests that the mean is higher than the median. This may be due to the presence of overhanging features on several strut surfaces, marked with the red ellipse in Fig. 7E, which can result in an exceptionally high value of R_a . Sample P360-T30 has the greatest R_a value of $25.45 \mu\text{m}$, which is 47 % higher than the lowest R_a value of $17.31 \mu\text{m}$ for sample P280-T30. Samples with a higher layer thickness (P280-T60 and P280-T90) exhibit higher R_a values of $22.10 \mu\text{m}$ and $20.72 \mu\text{m}$, respectively, compared to sample P280-T30 ($17.31 \mu\text{m}$), possibly due to the enhanced stair effect associated with higher layer thickness [2]. Section 3.1 discusses that an increase in layer thickness leads to a lack of fusion and deficiency in heat energy promotes the formation of rough surfaces due to partially molten powders attached to the strut's surface [1]. Similarly, sample P210-T30 has a high R_a value of 21.23 due to the lack of fusion. Despite the lower layer thickness of sample P280-T60, it has a slightly higher R_a value than sample P280-T90, possibly due to its greater strut thickness ($357 \mu\text{m}$) compared to sample P280-T90 ($344 \mu\text{m}$). The R_a value is the mean deviation of the surface profile from the mean profile, and the absolute value for the profile deviation of thicker struts appears to be greater than that of the thinner strut. In the same context, the R_a

value of sample P360-T30 (25.45 μm) can be explained by its greatest strut thickness (386 μm) among the lattice structures. To facilitate a more accurate comparison of R_a values, we calculated the ratios of R_a to strut thickness for each sample and presented them in Fig. 8B. The ratios for four lattices, excluding P280-T30, ranged from 0.06 to 0.066, which were similar to each other. However, sample P280-T30 had a significantly lower ratio of R_a to strut thickness of 0.048, corroborating the findings from the qualitative analysis. The R_a value and the ratio of R_a to strut thickness provide insight into the severity of surface roughness in lattice structures. By comparing the ratio of R_a to strut thickness, it can be deduced that the surface roughness of sample P280-T30 is substantially lower than that of the other samples, which have similar levels of surface roughness.

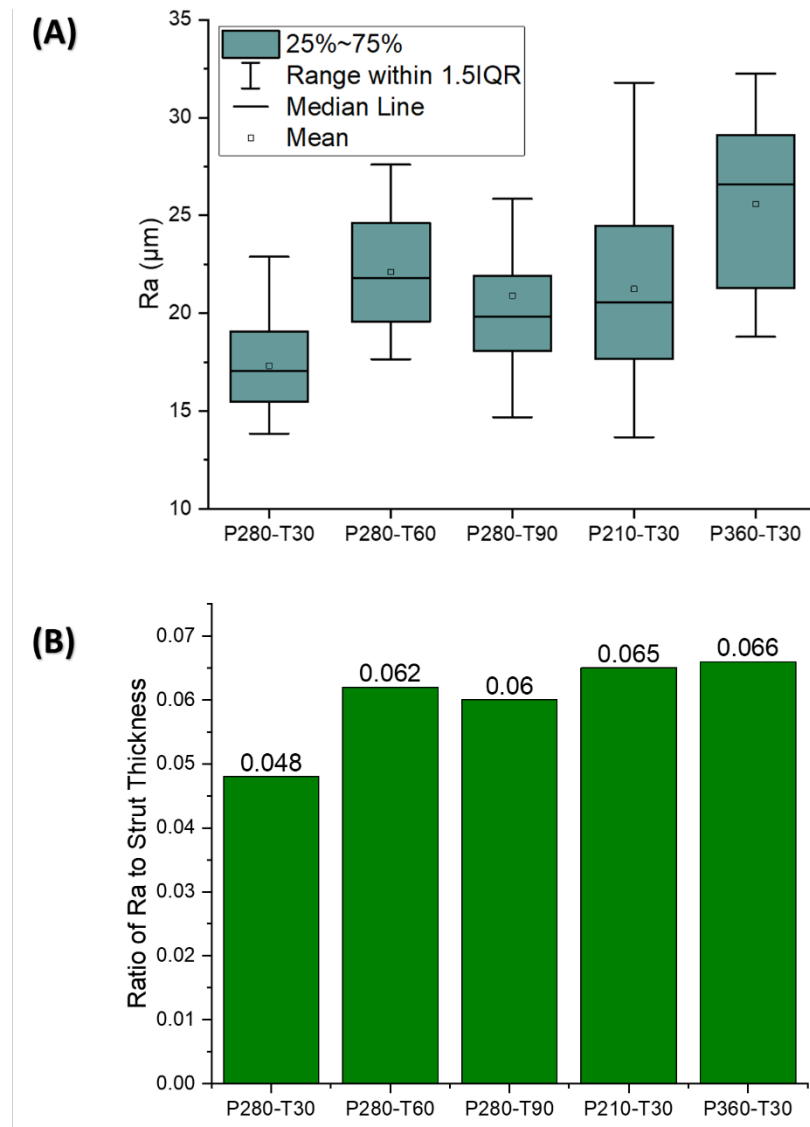


Fig.8. (A) Statistical data of R_a values demonstrated using Box and Whisker diagram and (B) a bar graph for the ratio of R_a to strut thickness.

By conducting a comprehensive CT scan analysis of the diamond lattice coupons, this study has been able to assess the manufacturing defects, such as geometrical discrepancies, internal porosity, and surface roughness. Among the samples, P280-T60 and P360-T30 have thick struts and nodes with low internal porosity, making them potentially outstanding in terms of manufacturing defects (Fig.9). However, these samples also have high surface roughness, which can be detrimental to the fatigue performance. The results show that laser power has a more significant impact on manufacturing defects compared to layer thickness. The internal porosity is highly sensitive to the change in process parameters, and the strut thickness shows a positive linear correlation with the laser power and a negative linear correlation with layer thickness. However, the effect of the process parameter on surface roughness remains unclear. Future work could investigate changes in roughness in different orientations along the strut.

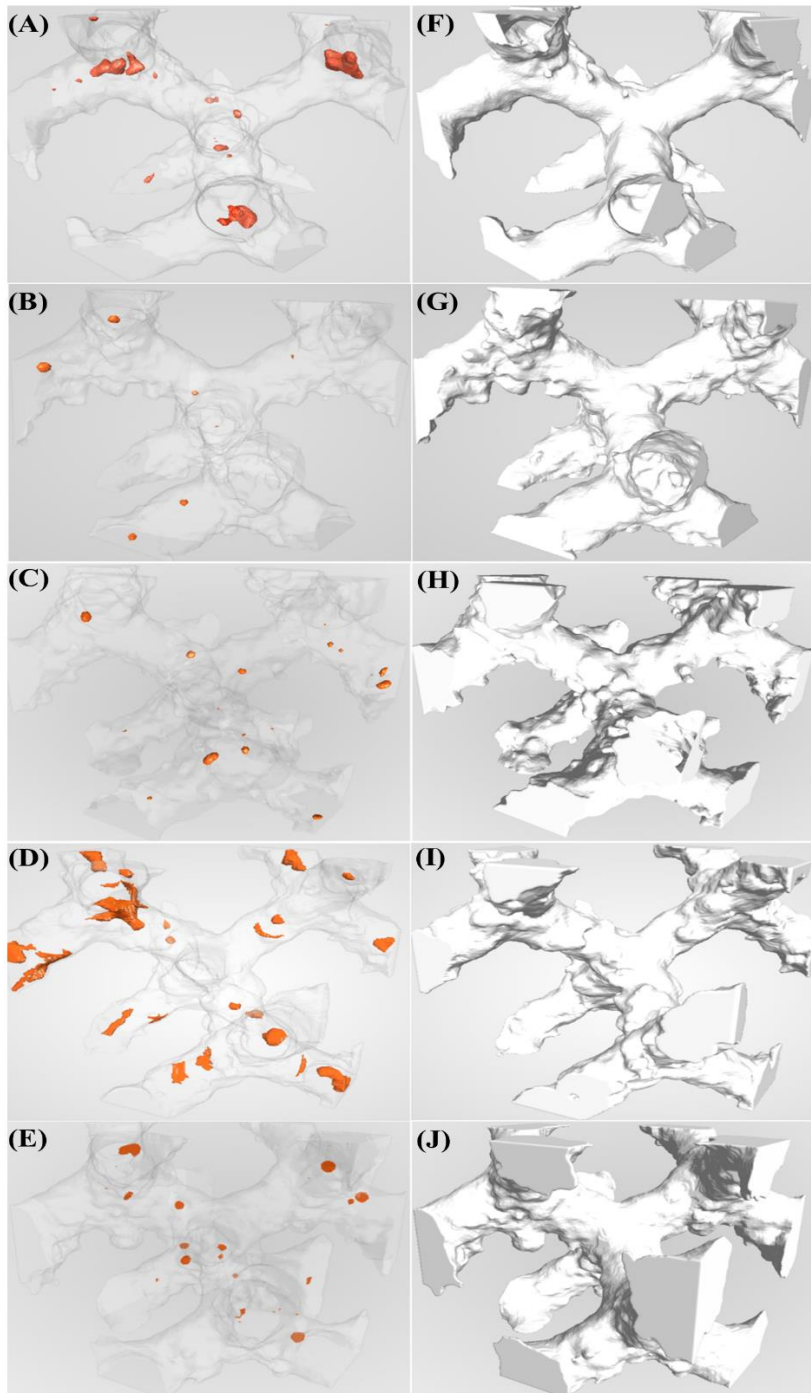


Fig.9. Internal porosity analysis, marked as orange color, on subsection of lattice structure (A) P280-T30, (B) P280-T60 (C) P280-T90, (D) P210-T30, and (E) P360-T30 and surface roughness mesh of subsection of lattice structure (F) P280-T30, (G) P280-T60, (H)P280-T90, (I) P210-T30, and (J) P360-T30

4 Conclusion

This study has provided insights into the influence of process parameters, specifically laser power and layer thickness, on the manufacturing defects of micro-strut lattice coupons. The results demonstrate that the parameters recommended to be optimal for solid materials found in the literature [11] are not necessarily optimal for lattice structures. In this work, we demonstrated that reduced porosity is found at higher layer thickness values, and further optimisation could be valuable to reduce porosity while also improving surface roughness. CT imaging was demonstrated to be a valuable approach for quantifying both the porosity and roughness of lattice structures for this purpose, with future work possible in evaluating lattice struts at a higher resolution or evaluating different orientations of roughness as a function of process parameters. Optimising and controlling process parameters can effectively improve the quality of micro-strut lattice structures, providing better performance, which opens up new possibilities for their application in various fields.

Reference

1. I. Yadroitsev, I. Yadroitsava, A. Du Plessis, E. Macdonald, *Fundamentals of Laser Powder Bed Fusion of Metals* (2021), doi: 20.1016/j.aime.2022.100070
2. M. Benedetti, A. du Plessis, R. O. Ritchie, M. Dallago, S. M. J. Razavi, and F. Berto, "Architected cellular materials: A review on their mechanical properties towards fatigue-tolerant design and fabrication," *Materials Science and Engineering R: Reports*, **144** (2021), doi: 10.1016/j.mser.2021.100606.
3. A. du Plessis, N. Razavi, M. Benedetti, S. Murchio, M. Leary, M. Watson, D. Bhate, F. Berto, "Properties and applications of additively manufactured metallic cellular materials: A review," *Progress in Materials Science*, **125**. (2022), doi: 10.1016/j.pmatsci.2021.100918.
4. D. Mahmoud, K. S. Al-Rubaie, and M. A. Elbestawi, "The influence of selective laser melting defects on the fatigue properties of Ti6Al4V porosity graded gyroids for bone implants," *Int J Mech Sci*, **193** (2021), doi: 10.1016/j.ijmecsci.2020.106180.
5. H. Gong, K. Rafi, H. Gu, G. D. J. Ram, T. Starr, and B. Stucker, "Influence of defects on mechanical properties of Ti-6Al-4V components produced by selective laser melting and electron beam melting," *Mater Des*, **86**, pp. 545–554 (2015), doi: 10.1016/j.matdes.2015.07.147.
6. G. Kasperovich, J. Haubrich, J. Gussone, and G. Requena, "Correlation between porosity and processing parameters in TiAl6V4 produced by selective laser melting," *Mater Des*, **105**, pp. 160–170 (2016) doi: 10.1016/j.matdes.2016.05.070.
7. D. S. Egan and D. P. Dowling, "Influence of process parameters on the correlation between in-situ process monitoring data and the mechanical properties of Ti-6Al-4V non-stochastic cellular structures," *Addit Manuf*, **30** (2019), doi: 10.1016/j.addma.2019.100890.
8. J. C. Fox, S. P. Moylan, and B. M. Lane, "Effect of Process Parameters on the Surface Roughness of Overhanging Structures in Laser Powder Bed Fusion Additive Manufacturing," in *Procedia CIRP*, Elsevier B.V (2016), doi: 10.1016/j.procir.2016.02.347.
9. A. Du Plessis, I. Yadroitsev, I. Yadroitsava, and S. G. Le Roux, "X-Ray Microcomputed Tomography in Additive Manufacturing: A Review of the Current Technology and Applications," *3D Print Addit Manuf*, **5**, 3, pp. 227–247 (2018), doi: 10.1089/3dp.2018.0060.

10. C. Yan, L. Hao, A. Hussein, and D. Raymont, "Evaluations of cellular lattice structures manufactured using selective laser melting," *Int J Mach Tools Manuf*, **62**, pp. 32–38 (2012), doi: 10.1016/j.ijmachtools.2012.06.002.
11. A. du Plessis, "Effects of process parameters on porosity in laser powder bed fusion revealed by X-ray tomography," *Addit Manuf*, **30** (2019) , doi: 10.1016/j.addma.2019.100871.
12. A. du Plessis, S. M. J. Razavi, and F. Berto, "The effects of microporosity in struts of gyroid lattice structures produced by laser powder bed fusion," *Mater Des*, **194**, (2020), doi: 10.1016/j.matdes.2020.108899.
13. A. du Plessis, S. G. le Roux, and A. Guelpa, "The CT Scanner Facility at Stellenbosch University: An open access X-ray computed tomography laboratory," *Nucl Instrum Methods Phys Res B*, **384**, pp. 42–49, (2016), doi: 10.1016/j.nimb.2016.08.005.
14. Y. L. Tee, J. R. Black, and P. Tran, "Virtual characterisation of porcupine quills using X-ray micro-CT", *Virtual Phys Prototyp*, **18**, 1, 2023, doi: 10.1080/17452759.2022.2126377.
15. N. Otsu, "A Threshold Selection Method from Gray-Level Histograms," in *IEEE Transactions on Systems, Man, and Cybernetics*, **9**, 1, pp. 62-66, Jan. 1979, doi: 10.1109/TSMC.1979.4310076.
16. R. N. Oosterbeek and J. R. T. Jeffers, "StrutSurf: A tool for analysis of strut morphology and surface roughness in additively manufactured lattices," *SoftwareX*, **18** (2022), doi: 10.1016/j.softx.2022.101043.